Two-Stage Collapse of Unimolecular Micelles with Double Thermoresponsive Coronas

Jian Xu,† Shizhong Luo,‡ Wenfang Shi,† and Shiyong Liu*,†,‡

The Hefei National Laboratory for Physical Sciences at Microscale, Hefei, Anhui, China; and Department of Polymer Science and Engineering, University of Science and Technology of China, Hefei, Anhui, China

Received August 20, 2005. In Final Form: October 8, 2005

Phase transition behavior of unimolecular dendritic three-layer nanostructures with dual thermoresponsive coronas is studied. Successive reversible addition-fragmentation transfer (RAFT) polymerizations of *N*-isopropylacrylamide (NIPAM) and 2-(dimethylamino)ethyl methacrylate (DMA) were conducted using fractionated fourth-generation hyperbranched polyester (Bolton H40) based macroRAFT agent. At lower temperatures (<20 °C), dendritic macromolecules *H40*-poly(*N*-isopropylacrylamide)-poly(2-(dimethylamino)ethyl methacrylate) (*H40*−PNIPAM-PDMA) exist as unimolcular core−shell-corona nanostructures with hydrophobic *H40* as the core, swollen PNIPAM as the inner shell, and swollen PDMA as the corona. PNIPAM and PDMA homopolymers undergo phase transitions at their lower critical solution temperatures (LCST), which are found to be 32 °C for PNIPAM and 40−50 °C for PDMA, respectively. Upon continuously heating through the LCSTs of PNIPAM and PDMA, such dendritic unimolecular micelles exhibit two-stage thermally induced collapse. This process is reversible with a two-stage reswelling upon cooling. Laser light scattering, micro-differential scanning calorimetry, and excimer fluorescence measurements are used to investigate the double phase transitions.

Introduction

The interest in stimuli-responsive polymers has exponentially increased due to their promising potential in a variety of applications for the biomedical fields.[1,2] Among them, temperature and pH-responsive mechanisms have been extensively investigated because they are relatively convenient and effective stimuli in many applications.[2] Poly(*N*-isopropyl acrylamide) (PNIPAM) undergoes a phase transition at its lower critical solution temperature (LCST) of 32 °C, and it has been widely studied as a polymer potentially useful for targeted drug delivery.[1] Besides PNIPAM, other *N*-substituted poly(acrylamide)[3] or poly(2-(dimethylamino)ethyl methacrylate) (PDMA) undergo the same phase transition below and above their LCST, which was found to be 33 °C for poly(*N*,*N*-diethylacrylamide)[4] and 40−50 °C for PDMA depending on its molecular weight.[5−7]

Up to now, studies on stimuli-responsive polymers mainly deal with amphiphilic and double hydrophilic block copolymers (DHBCs).[8] DHBCs can self-assemble and form micellar or "reverse" micellar structures in water if external conditions such as temperature, pH, and ionic strength are finely tuned.[8−13] Block copolymers micelles usually have a large aggregation number and their structure is not static.[14−20] There exist dynamic exchange between micelles and unimers. So they tend to be destroyed under shear forces, dilution, and salinity fluctuations. Chemical cross-linking of the micellar core or shell can be utilized to address the problem of insufficient stability of block copolymer micelles.[21−28] An alternate and facile approach is to prepare unimolecular micelles. Amphiphiles that are tethered to a multifunctional core, such as dendritic macromolecules and heteroarm star copolymers, have been synthesized and investigated as unimolecular micelles.[29−35] Compared to conventional block copolymer micelles, dendritic macromolecules or polymeric

* To whom correspondence should be addressed. E-mail: sliu@ustc.edu.cn.
† University of Science and Technology of China.
‡ The Hefei National Laboratory for Physical Sciences at Microscale.

(1) Riess, G. *Prog. Polym. Sci.* **2003**, *28*, 1107.
(2) Gil, E. S.; Hudson, S. A. *Prog. Polym. Sci.* **2004**, *29*, 1173.
(3) Ito, S.; Fujishige, S. *Kobunshi Ronbunshu* **1989**, *46*, 437.
(4) (a) Idziak, I.; Avoce, D.; Lessard, D.; Gravel, D.; Zhu, X. X. *Macromolecules* **1999**, *32*, 1260. (b) Maeda, Y.; Nakamura, T.; Ikeda, I. *Macromolecules* **2002**, *35*, 10172.
(5) (a) Butun, V.; Billingham, N. C.; Armes, S. P. *Chem. Commun*. **1997**, 671. (b) Lee, A. S.; Gast, A. P.; Butun, V.; Armes, S. P. *Macromolecules* **1999**, *32*, 4302.
(6) Butun, V.; Armes, S. P.; Billingham, N. C. *Polymer* **2001**, *42*, 5993.
(7) Vamvakaki, M.; Billingham, N. C.; Armes, S. P. *Macromolecules* **1999**, *32*, 2088.
(8) Cölfen, H. *Macromol. Rapid Commun.* **2001**, *22*, 219.
(9) Gohy, J. F.; Lohmeijer, B. G. G.; Varshney, S. K. *Macromolecules* **2002**, *35*, 9748.
(10) Hadjikallis, G.; Hadiyannakou, S. C.; Vamvakaki, M. *Polymer* **2002**, *43*, 7269.
(11) Andre, X.; Zhang, M. F.; Muller, A. H. E. *Macromol. Rapid. Commun.* **2005**, *26*, 558.
(12) Rodriguez-Hernandez, J.; Lecommandoux, S. *J. Am. Chem. Soc.* **2005**, *127*, 2026−2027.
(13) Arotcarena, M.; Heise, B.; Ishaya, S.; Laschewsky, A. *J. Am. Chem. Soc.* **2002**, *124*, 3787.
(14) Hamley, I. W. In *The Physics of Block Copolymers*; Oxford University Press: Oxford, U.K., 1998; p 131.
(15) Zhang, L.; Eisenberg, A. *Science* **1995**, *268*, 1728.
(16) Zhang, L.; Eisenberg, A. *J. Am. Chem. Soc.* **1996**, *118*, 3168.
(17) Shen, H.; Eisenberg, A. *Macromolecules* **2000**, *33*, 2561.
(18) Ding, J.; Liu, G. *Macromolecules* **1997**, *30*, 655.
(19) Discher, B. M.; Won, Y.; Ege, D. S.; Lee, J. C.-M.; Bates, F. S.; Discher, D. E.; Hammer, D. A. *Science* **1999**, *284*, 1143.
(20) Jenekhe, S. A.; Chen, X. L. *Science* **1998**, *279*, 1903; *283*, 372.
(21) Thurmond, K. B.; Kowalewski, T.; Wooley, K. L. *J. Am. Chem. Soc.* **1996**, *118*, 7239.
(22) Thurmond, K. B.; Kowalewski, T.; Wooley, K. L. *J. Am. Chem. Soc.* **1997**, *119*, 6656.
(23) Wooley, K. L. *J. Polym. Sci., Part A: Polym. Chem*. **2000**, *38*, 1397.
(24) Wang, X. S.; Arsenault, A.; Ozin, G. A.; Winnik, M. A.; Manners, I. *J. Am. Chem. Soc*. **2003**, *125*, 12686.
(25) Underhill, R. S.; Liu, G. *Chem. Mater*. **2000**, *12*, 2082.
(26) Stewart, S.; Liu, G. *Chem. Mater*. **1999**, *11*, 1048.
(27) Bütün, V.; Billingham, N. C.; Armes, S. P. *J. Am. Chem. Soc.* **1998**, *120*, 11818.
(28) Liu, S.; Weaver, J. V. M.; Save, M.; Armes, S. P. *Langmuir* **2002**, *18*, 8350.
(29) Tomalia, D. A.; Berry, V.; Hall, M.; Hedstrand, D. M. *Macromolecules* **1987**, *20*, 1164.
(30) Hawker, C. J.; Wooley, K. L.; Frechét, J. M. J. *J. Chem. Soc., Perkin Trans. 1* **1987**, *20*, 1164.
(31) Pispas, S.; Poulos, Y.; Hadjichristidis, N. *Macromolecules* **1998**, *31*, 4177.
(32) Semenov, A. N.; Vlassopoulos, D.; Fytas, G.; Vlachos, G.; Fleischer, G.; Roovers, J. *Langmuir* **1999**, *15*, 358.

10.1021/la0522707 CCC: $33.50
Published on Web 12/31/2005

unimolecular micelles offer much higher stability in aqueous solution since they contain only covalently linked branching points.

So it would offer more advantages if we combine the properties of dendritic or starlike core−shell macromolecules with stimuli-responsive DHBCs. In aqueous solution, it will behave like typical DHBCs and their shape and size will respond to external stimuli; most importantly, they are unimolecular and structurally stable. Studies of stimuli-responsive dendritic core−shell macromolecules are still rare. Kimura et al. prepared the DAB−Am-32 poly(propylenimine) dendrimer having poly(*N*-isopropylacrylamide) armes as a temperature-sensitive host for cobalt phthalocyanins.[36] Thermoresponsive dendritic polymers with PNIPAM as the shell have also been synthesized from a second generation dendrimer recently.[37] Interestingly, Kono et al. reported that the introduction of isobutyramide (IBAM) groups to the chain ends of poly(amidoamine) or poly(propylenimine) dendrimers could successfully produce a temperature-sensitive water solubility to the dendrimers.[38] Haag et al. has prepared pH-responsive nanocarriers by selective shell functionalization of hyperbranched polyglycerol.[39,40] Richtering et al. reported the doubly thermoresponsive core−shell microgels consisting of an poly(*N*-isopropylacrylamide) core and poly(*N*-isopropylmethacrylamide) shell. Both the core and shell are cross-linked and have separate LCSTs.[41,42] As far as we know, there have been no reports on dendritic core−shell macromolecules with double stimuli-responsive properties.

Herein we report the first preparation of unimolecular dendritic core−shell-corona nanostructures with dual thermoresponsive coronas based on a commercially available hyperbranched polymer.[43−47] Two successive reversible addition-fragmentation transfer (RAFT) polymerizations of NIPAM and DMA were conducted using a dendritic macroRAFT agent. The resulting dendritic H40−PNIPAM-PDMA is then investigated as unimolecular micelles with double thermoresponsive coronas. We show that this novel three-layer dendritic unimoelcular nanostructure exhibits double thermal phase transitions. In dilute aqueous solutions, they undergo reversible two-stage collapse or reswelling upon heating or cooling.

Experimental Section

Materials. Hyperbranched polyester Boltorn H40 was obtained from Perstorp Polyols AB. It was further purified and fractionated with a typical 20% yield using procedures reported by Tsukruk et al.[43−45] Boltorn H40 as an ideal dendrimer would theoretically have 64 primary hydroxyl groups and a molar mass of 7316 g mol^{-1}, and its ideal structure is shown in Scheme 1. SEC analysis of the fractionated *H40* indicated a M_n of 6500 g mol^{-1} and a polydispersity of 1.40. We denote the purified and fractionated hyperbranched polyester as *H40* here. According to Tsukruk et al.,[43] the degree of branching of *H40* was 0.4, and the average number of monomeric units (the degree of polymerization) was 60.

Scheme 1. Schematic Representation of the Ideal Structure of Fourth-generation Hyperbranched Polyester *H40*

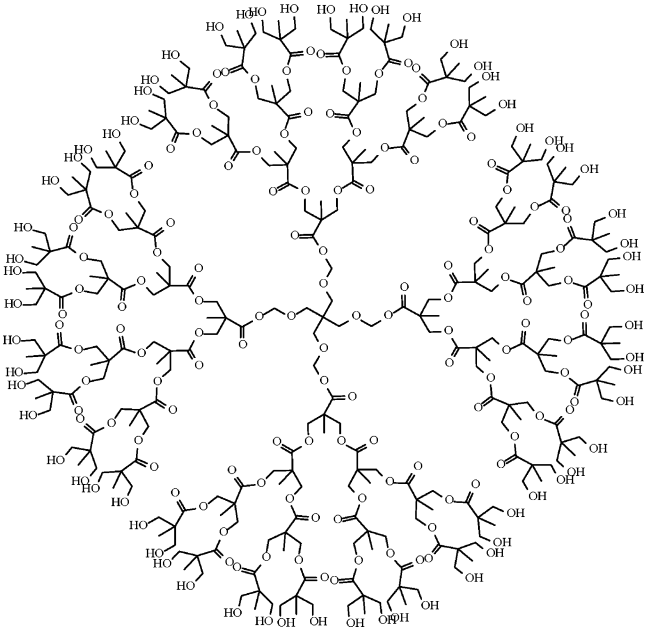

2-(Dimethylamino)ethyl methacrylate (DMA) was passed through basic alumina columns, then vacuum-distilled from CaH_2, and stored at −20 °C prior to use. *N*-Isopropylacrylamide (NIPAM) was purified by recrystallization in a benzene/*n*-hexane mixture. THF was distilled over sodium/benzophenone. Other reagents were used as received.

Sample Preparation. A general approach to prepare *H40*−PNIPAM and *H40*−PNIPAM-PDMA was shown in Scheme 2. The experimental details are described below.

Synthesis of Maleic Anhydride Modified H40. H40 (3.658 g, 0.5 mmol) was dissolved in anhydrous THF (200 mL), and then maleic anhydride (MAh) (10 g, 100 mmol) was added. The mixture was stirred at 80 °C for 24 h. Most of the solvent was removed by rotary evaporation prior to precipitation into a 10-fold excess of ether. *H40* with terminal ester groups was further purified by precipitation into petroleum ether from THF three times to remove any unreacted MAh. The resulting *H40*-MAh was dried overnight in a vacuum oven at 30 °C.[37]

Synthesis of Dithiobenzoic Acid (DTBA). The Grignard reagent prepared from bromobenzene (10.5 g) and magnesium (2.5 g) in dried THF (100 mL) was reacted with carbon disulfide (6.0 g) in THF (50 mL) at 0 °C for 2 h. The mixture was decomposed with ice-cold dilute hydrochloric acid (50 mL), and most of the THF was removed by rotary evaporation. The organic layer was separated and extracted with ice-cold 10% sodium hydroxide solution (30 mL × 3). The alkaline solution was washed with diethyl ether three times, acidified with ice-cold 10% hydrochloric acid solution, and finally extracted with diethyl ether. The ether solution was washed with distilled water three times. After evaporation of the solvent, pure DTBA was obtained in 73.6% yield. ^{1}H NMR (300 MHz, $CDCl_3$): δ 6.5 (s, 1H, −C(=S)S*H*), δ 7.0−7.9 (m, 5H, aromatic *H*).

Synthesis of H40 macroRAFT Agent. A solution of *H40*-MAh (2.726 g, 0.2 mmol) and DTBA (6.16 g, 40 mmol) in dried THF (100 mL) was sealed in a degassed tube, and the reaction of DTBA with *H40*-MAh was carried out at 65 °C for 24 h. *H40* capped with dithiobenzoate groups was obtained by precipitation into excess diethyl ether from THF to remove any un-reacted DTBA. The resulting product was dried in a vacuum oven at room temperature.

(33) Voulgaris, D.; Tsitsilianis, C.; Esselink, F. J.; Hadziioannou, G. *Polymer* **1998**, *25*, 6429.
(34) Yoo, M.; Heise, A.; Hedrick, J. L.; Miller, R. D.; Frank, C. W. *Macromolecules* **2003**, *36*, 268.
(35) Teertstra, S. J.; Gauthier, M. *Prog. Polym. Sci.* **2004**, *29*, 277.
(36) Kimura, M.; Kato, M.; Muto, T.; Hanabusa, K.; Shirai, H. *Macromolecules* **2000**, *33*, 1117.
(37) You, Y. Z.; Hong, C. Y.; Pan, C. Y.; Wang, P. H. *Adv. Mater*. **2004**, *16*, 1953.
(38) Haba, Y.; Harada, A.; Takagishi, T.; Kono, K. *J. Am. Chem. Soc*. **2004**, *126*, 12760.
(39) Krämer, M.; Stumbé, J.-F.; Türk, H.; Krause, S.; Komp, A.; Delineau, L.; Prokhorova, S.; Kautz, H.; Haag, R. *Angew. Chem., Int. Ed.* **2002**, *41*, 4252.
(40) Niwa, M.; Higashizaki, T.; Higashi, N. *Tetrahedron* **2003**, *59*, 4011.
(41) Berndt, I.; Richtering, W. *Macromolecules* **2003**, *36*, 8780.
(42) Berndt, I.; Pedersen, J. S.; Richtering, W. *J. Am. Chem. Soc*. **2005**, *127*, 9372.
(43) Ornatska, M.; Peleshanko, S.; Genson, K. L.; Rybak, B.; Bergman, K. N.; Tsukruk, V. V. *J. Am. Chem. Soc*. **2004**, *126*, 9675.
(44) Ornatska, M.; Peleshanko, S.; Rybak, B.; Holzmueller, J.; Tsukruk, V. V. *Adv. Mater*. **2004**, *16*, 2206.
(45) Ornatska, M.; Bergman, K. N.; Rybak, B.; Peleshanko, S.; Tsukruk, V. V. *Angew. Chem., Int. Ed.* **2004**, *43*, 5246.
(46) Arce, E.; Nieto, P. M.; Diaz, V.; Castro, R. G.; Bernad, A.; Rojo, J. *Bioconjugate Chem.* **2003**, *14*, 817.
(47) Jesberger, M.; Barner, L.; Stenzel, M. H.; Malmström, E.; Davis, T. P.; Barner-Kowolli. *J. Polym. Sci.: Part A: Polym. Chem*. **2003**, *41*, 3847.

Scheme 2. Reaction Scheme for the Preparation of *H40*-PNIPAM and *H40*-PNIPAM-PDMA Dendritic Macromolecules

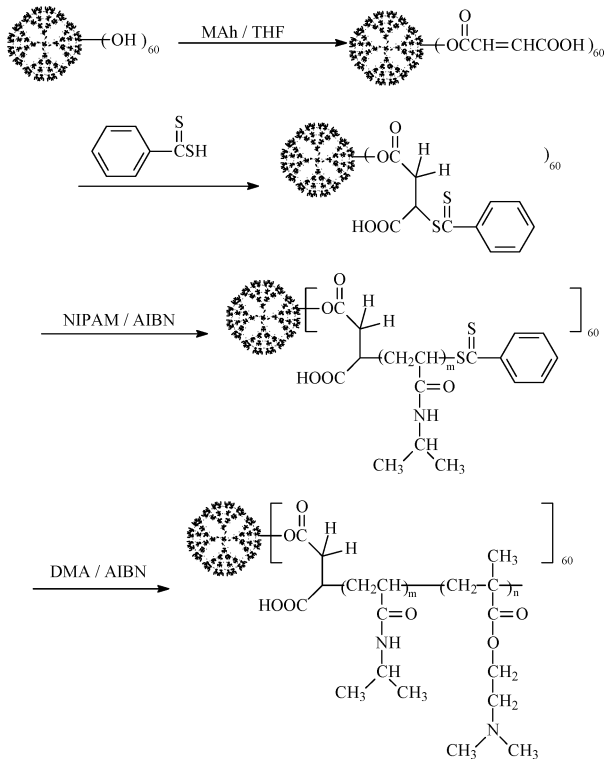

Synthesis of [4-(1-Pyrenyl)butyl] Acrylate. Acryloyl chloride (1.0 mL, 12.3 mmol) was added to a stirred solution of 1-pyrenebutanol (1.0 g, 3.6 mmol) and triethylamine (1.5 g, 15 mmol) in 20 mL of dichloromethane over a period of 1 h under nitrogen at 0 °C. The reaction mixture was stirred overnight at room temperature in the dark; it was diluted with chloroform (50 mL) and filtered to remove triethylamine hydrochloride formed during the reaction. The filtrate was washed with 1 M HCl, brine, 1 M $NaHCO_3$, and brine, successively. The organic layer was dried over magnesium sulfate, filtered, and evaporated under reduced pressure to give a yellow product.

Synthesis of H40−PNIPAM. The general procedure for synthesizing *H40*−PNIPAM was as follows. A glass ampule was charged with *H40* macroRAFT agent, AIBN, and NIPAM in THF; it was then degassed by three freeze−thaw cycles and sealed under vacuum. The polymerization was carried out at 80 °C for 12 h. The mixture was precipitated into anhydrous diethyl ether twice. The product was collected by filtration and then dried in a vacuum oven at room temperature.

Synthesis of H40−PNIPAM-PDMA. The general procedure for synthesizing *H40*−PNIPAM-PDMA was as follows. A glass ampule was charged with *H40*−PNIPAM macroRAFT agent prepared as described above, AIBN, and DMA in THF; it was then degassed by three freeze−thaw cycles and sealed under vacuum. The polymerization was carried out at 60 °C for 8 h. The final product was obtained by precipitation into anhydrous diethyl ether twice, collected by filtration, and then dried under vacuum at room temperature. *H40*−PNIPAM-PDMA(Py) was synthesized by RAFT copolymerization of DMA and 4-(1-pyrenyl)butyl] acrylate using *H40*−PNIPAM as macroRAFT agent.

Characterization. *Nuclear Magnetic Resonance (NMR) Spectroscopy.* All ^{1}H NMR spectra were recorded using a Bruker 300 MHz spectrometer. *H40* and *H40* based macroRAFT agent were analyzed in *d*-DMSO, *H40*−PNIPAM and *H40*−PNIPAM-PDMA were analyzed either in *d*-DMSO or $CDCl_3$.

Size Exclusion Chromatography (SEC). Molecular weight distributions were determined by SEC using a series of three linear Styragel columns HT3, HT4, and HT5 and an oven temperature of 60 °C. Waters 1515 pump and Waters 2414 differential refractive index detector (set at 30 °C) was used. The eluent was DMF + 1 g/L BrLi at a flow rate of 1.0 mL/min.

Laser Light Scattering (LLS). A commercial spectrometer (ALV/DLS/SLS-5022F) equipped with a multi-tau digital time correlation (ALV5000) and a cylindrical 22 mW UNIPHASE He−Ne laser (λ_0 = 632 nm) as the light source was used. In static LLS, we can obtain the weight-average molar mass (M_w) and the *z*-average root-mean square radius of gyration ($\langle R_g^2\rangle^{1/2}$ or written as $\langle R_g\rangle$) of polymer chains in a dilute solution from the angular dependence of the excess absolute scattering intensity, known as Rayleigh ratio $R_{vv}(q)$, as

$$\frac{KC}{R_{vv}(q)} \approx \frac{1}{M_w}\left(1 + \frac{1}{3}\langle R_g^2\rangle q^2\right) + 2A_2C \qquad (1)$$

where $K = 4\pi^2 n^2 (dn/dC)^2/(N_A\lambda_0^4)$ and $q = (4\pi n/\lambda_0)\sin(\theta/2)$ with N_A, dn/dC, n, and λ_0 being the Avogadro number, the specific refractive index increment, the solvent refractive index, and the wavelength of the laser light in a vacuum, respectively; and A_2 is the second virial coefficient. Strictly speaking, here $R_{vv}(q)$ should be $R_{vu}(q)$ because there is no analyzer before the detector. However, the depolarized scattering of the solution studied is insignificant so that $R_{vu}(q) \sim R_{vv}(q)$. Also note that in this study, the sample solution for LLS was so dilute (1.0×10^{-6} g/mL) that the extrapolation of $C \rightarrow 0$ was not necessary, and the term $2A_2C$ in eq 1 can be neglected, the obtained M_w value is denoted as the apparent molecular weight, $M_{w,app}$.[48]

Specific refractive index increment, dn/dC, was determined by a precise differential refractometer at 632 nm.[49] For PNIPAM homopolymer in water, dn/dC values exhibit weak temperature dependence, which are 0.167 and 0.174 mL/g at 25 and 40 °C, respectively.[50] A dn/dC value of PDMA homopolymer in water is determined to be 0.151 mL/g at 25 °C. dn/dC values of PNIPAM and PDMA homopolymer are quite comparable, both blocks in *H40*-PNIPAM-PDMA are "visible" under LLS measurements and contribute to the overall scattering light intensities in proportion to their relative weight fractions. Due to the slight difference in dn/dC for PNIPAM and PDMA, the determined $\langle R_g\rangle$ and M_w should only be considered as "apparent" values because no correction is given. dn/dC of *H40*-PNIPAM in water is determined to be 0.154 mL/g at 15 °C. For *H40*-PNIPAM-PDMA in aqueous solution, their dn/dC values are determined to be 0.155, 0.157, and 0.161 mL/g at 15, 35, and 60 °C, respectively. The same dn/dC value of 0.155 mL/g is used for *H40*-PNIPAM-PDMA(Py) in water at 15 °C, assuming that the incorporation of 0.9 mol % pyrene monomer units into the PDMA outer corona has negligible effect on dn/dC. The above dn/dC values are then used in the determination of $M_{w,app}$ of *H40*-PNIPAM and *H40*-PNIPAM-PDMA at different temperatures.

In dynamic LLS, the Laplace inversion of each measured intensity−intensity-time correlation function $G^{(2)}(q,t)$ in the self-beating mode can lead to a line-width distribution $G(\Gamma)$. For a pure diffusive relaxation, Γ is related to the translational diffusion coefficient D by $(\Gamma/q^2)_{C\rightarrow 0, q\rightarrow 0} \rightarrow D$, or further to the hydrodynamic radius R_h via the Stokes−Einstein equation, $R_h = (k_BT/6\pi\eta_0)/D$, where k_B, T, and η_0 are the Boltzmann constant, the absolute temperature, and the solvent viscosity, respectively.

Micro-Differential Scanning Calorimetry (Micro-DSC). The copolymer solutions were measured by a VP-DSC microcalorimeter (MicroCal Inc) at an external pressure of 180 kPa. The cell volume was 0.157 mL. The heating rate was 1.0 °C/min, and the instrument response time was set at 5.6 s. All the micro-DSC data were corrected for instrument response time and analyzed using the software in the calorimeter.

Fluorescence Measurements. Fluorescence spectra were recorded using a JASCO FP-6200 spectrofluoriometer. The temperature of the water-jacketed cell holder was controlled by a programmable circulation bath. The slit widths were set at 5 nm for both the excitation

(48) Wu, C.; Zhou, S. Q. *Macromolecules* **1995**, *28*, 8381.
(49) Wu, C.; Xia, K. Q. *Rev. Sci. Instrum.* **1994**, *65*, 587.
(50) Gao, J.; Wu, C. *Macromolecules* **1997**, *30*, 6873.

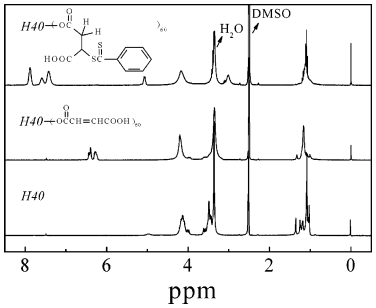

Figure 1. ^{1}H NMR spectra of *H40*, *H40*-MAh, and *H40* macroRAFT agent in *d*-DMSO.

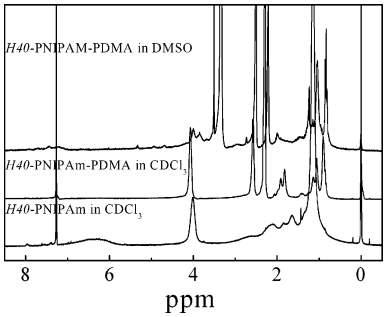

Figure 2. ^{1}H NMR spectra of *H40*−PNIPAM in $CDCl_3$ and *H40*−PNIPAM-PDMA in *d*-DMSO and $CDCl_3$.

and the emission. In a 1 cm cell, the samples were heated slowly with the heating rate of 0.1 °C/min. The excimer-to-monomer ratio was calculated as the ratio of the emission intensity at 480 nm to that of the emission at 373 nm.

Atomic Force Microscopy. Multimode AFM instrument (Digital Instrucments, Santa Barbara) was operated in the tapping mode. Aqueous solution of *H40*−PNIPAM-PDMA at 1.0×10^{-3} g/mL was spin-coated at 300 rpm onto freshly cleaved mica at room temperature.

Results and Discussion

Synthesis of H40−PNIPAM and H40−PNIPAM-PDMA. A general approach to prepare *H40*−PNIPAM and *H40*−PNIPAM-PDMA was shown in Scheme 2. It is worth noting that the numbers as well as chemical structure described in Scheme 2 and in the following text should be considered only as averaging for irregular hyperbranched architectures as was discussed in numerous publications specifically devoted to this issue.[51−53]

Synthesis of H40 macroRAFT Agent. The *H40* macroRAFT agent was prepared via a two-step approach.[37] Hydroxyl-terminated *H40* was reacted with MAh in THF. Figure 1 shows the ^{1}H NMR spectra of *H40* and *H40*-MAh, respectively. Compared to the spectrum of *H40*, the complete esterification of peripheral hydroxyl groups of *H40* was qualitatively evidenced by the disappearance of signals at $\delta = 3.5$ ppm, which is due to methylene protons of primary $-CH_2OH$ groups. In the spectrum of *H40*-MAh, the signals at $\delta = 4.2$ and 6.1−6.5 ppm are corresponding to all of the ester methylene protons of *H40*-MAh and protons of double bonds from the maleic acid monoester groups. From the intensity ratio of these two peaks, the number of maleic acid monoester groups per *H40*-MAh is calculated to be ∼60, considering that the average number of monomeric units (the degree of polymerization) of *H40* was 60 as revealed by Tsukruk et al.[43] Due to the strong acidity of DTBA compared to maleic acid monoester, it can readily react with the double bond to give the corresponding *H40* based macroRAFT agent. The successful preparation of *H40* macroRAFT agent was confirmed by the complete disappearance of signal at $\delta = 6.1-6.5$ ppm and the appearance of new signals at $\delta = 7.9$, 7.6, and 7.4 ppm, ascribed to the ortho-, para-, and meta-position protons of dithiobenzoyl group, respectively, although new signals at $\delta = 5.1$ and 3.0 ppm (peak area ratio ∼ 1:2) are ascribed to the methine proton next to the dithiobenzoyl group and the methylene protons next to the MAh ester carbonyl groups.

Synthesis of H40−PNIPAM and H40−PNIPAM-PDMA. RAFT polymerization of NIPAM was performed in a sealed glass ampule under vacuum using *H40* macroRAFT agent to prepare dendritic macromolecules with PNIPAM as the first layer and *H40* as the dendritic core. NIPAM can be considered as a neutral monomer, whereas DMA is a weakly basic one.[1,5−6] Direct mixing of *H40* macroRAFT agent with DMA monomer in THF results in precipitation. This is due to the presence of peripheral carboxyl groups on *H40* macroRAFT agent; there exist acid−base interactions between carboxyl groups and tertiary amine groups of DMA units. Pan et al. have investigated the RAFT polymerization of NIPAM from a second generation dendrimer and found that RAFT polymerization of NIPAM can be carried out in a controlled manner.[37] Here we did not study in detail the kinetics of RAFT polymerization of NIPAM using *H40* macroRAFT agent. The *H40* macroRAFT agent is not soluble in $CDCl_3$, while *H40*−PNIPAM is readily soluble in $CDCl_3$. The good solubility of *H40*−PNIPAM in $CDCl_3$ indirectly proves the core−shell structure with *H40* as the dendritic core and PNIPAM as the shell. ^{1}H NMR spectrum of *H40*−PNIPAM in $CDCl_3$ shown in Figure 2 reveals the presence of characteristic signals of PNIPAM at $\delta = 5.8-7.0$, 4.0, and 1.2 ppm. We did not observe any signals due to the *H40* dendritic core, which is not soluble in $CDCl_3$. The signals at $\delta = 5.1$ ppm, ascribed to the methine proton next to the dithiobenzoyl group in the macroRAFT agent, completely disappeared after the polymerization of NIPAM, so we can qualitatively tell that all of the surface dithiobenzoyl groups in the macroRAFT agent participated in the polymerization of NIPAM. SEC analysis in DMF of *H40*−PNIPAM gives a symmetric elution peak with a number average molecular weight (M_n) of 4.75×10^5 g mol^{-1} and a polydispersity of 1.22, whereas *H40* itself has a M_n of 6500 g mol^{-1} and polydispersity of 1.40. The relatively narrow polydispersity of *H40*−PNIPAM indicated that the RAFT polymerization of NIPAM using *H40* macroRAFT agent was conducted in a controlled manner. Due to the fact that SEC analysis uses linear polystyrene as standards and *H40*−PNIPAM take a dendritic conformation, SEC tends to underestimate the molecular weight, and static LLS is then used to determine the absolute molecular weight of *H40*−PNIPAM. The results were shown in Table 1. The weight averaged molecular weight, $M_{w,app}$, determined by LLS is 7.6×10^5 g mol^{-1}. The average degree of polymerization (DP) of grafted PNIPAM chains is thus calculated to be 110 considering that there are 60 PNIPAM chains are grown from each *H40* macroRAFT agent.

^{1}H NMR spectrum of *H40*−PNIPAM in $CDCl_3$ also reveals the presence of signals at $\delta = 7.9$, 7.6, and 7.4 ppm, which are ascribed to the dithiobenzoyl groups located at the PNIPAM chain ends because *H40* macroRAFT agent is not soluble in $CDCl_3$. Thus, *H40*−PNIPAM can be used as another macroRAFT agent to polymerize DMA. As stated previously, although *H40* macroRAFT agent cannot directly polymerize DMA due to solubility problems, mixed solutions of *H40*−PNIPAM and DMA monomer in THF are clear and show no precipitates formation. This indicated that, in *H40*−PNIPAM, surface carboxyl groups

(51) Claesson, H.; Malmstroem, E.; Johansson, M.; Hult, A. *Acta Polym.* **2002**, *43*, 3511.
(52) Zagar, E.; Zigon, M. *Macromolecules* **2002**, *35*, 9913.
(53) Hanselman, R.; Hoelter, D.; Frey, H. *Macromolecules* **1998**, *31*, 3790.

Table 1. Molecular Parameters of Dendritic Macromolecules Used in This Study

samples	DP of PNIPAM[a]	DP of PDMA[a]	M_n g mol^{-1}[b]	M_w/M_n	$M_{w,app}$ g mol^{-1}[c]
H40−PNIPAM	110	/	4.75×10^5	1.22	7.60×10^5
H40−PNIPAM-PDMA	110	320	1.57×10^6	1.15	3.74×10^6
H40−PNIPAM-PDMA(Py)	110	250	1.20×10^6	1.18	3.15×10^6

[a] Average degrees of polymerization (DP) of PNIPAM or PDMA block. [b] Determined by SEC using DMF + 1.0 g/L BrLi as eluent. [c] Determined in water by static LLS at 15 °C.

in H40 macroRAFT agent were located at the *H40*/PNIPAM interface, and PNIPAM shell now acts as a shielding layer. Polymerization of DMA using *H40*−PNIPAM as macroRAFT agent was again conducted in THF at 60 °C. A lower temperature was used as compared to the polymerization of NIPAM since the RAFT polymerization of DMA is faster and much higher conversion can be achieved. Figure 2 shows the ^{1}H NMR spectra of *H40*−PNIPAM-PDMA in $CDCl_3$ and *d*-DMSO, respectively. It is interesting to note that, although the PNIPAM inner layer is soluble in $CDCl_3$, *H40*−PNIPAM-PDMA in $CDCl_3$ only shows signals characteristic of PDMA outer layer. Possibly this is due to that PNIPAM chains are constrained between the insoluble H40 core and readily soluble PDMA outer layer, chain mobility of the PNIPAM inner layer is greatly restricted. In *d*-DMSO, all of the characteristic signals due to the *H40* core, PNIPAM, and PDMA layers can be clearly observed. This again confirmed that *H40*−PNIPAM-PDMA take a dendritic three-layer nanostructure.

SEC analysis of *H40*−PNIPAM-PDMA gives a M_n of 1.57×10^6 g mol^{-1} and a polydispersity of 1.15. Static LLS consistently gives a much higher value of $M_{w,app} \sim 3.74 \times 10^6$ g mol^{-1}. The DP of PDMA block is calculated to be 320, assuming that there are 60 PNIPAM-*b*-PDMA graft chains at the surface of the *H40* core. So the DPs of PNIPAM and PDMA of *H40*−PNIPAM-PDMA are 110 and 320, respectively. We have also synthesized *H40*−PNIPAM-PDMA(Py), where the PDMA block is selectively copolymerized with 4-(1-pyrenyl)butyl acrylate using *H40*−PNIPAM as macroRAFT agent. Based on the $M_{w,app}$ of 3.15×10^6 determined by static LLS, the DP of PNIPAM and PDMA in *H40*−PNIPAM-PDMA(Py) are calculated to be 110 and 250, respectively. The pyrene content determined by UV−vis absorption using 1-pyrenebutanol as a model compound is 0.9 mol % based on the DMA units; on average there are 2.2 pyrene units per PDMA block. The molecular parameters of *H40*−PNIPAM, *H40*−PNIPAM-PDMA and *H40*−PNIPAM-PDMA(Py) are listed in Table 1.

Thermally Induced Collapse of *H40*-PNIPAM. It is well-known that PNIPAM homopolymer undergoes a coil-to-globule phase transition in dilute aqueous solution at its LCST of ca. 32 °C.[1] PDMA homopolymer also exhibits LCST phase transition. The LCST of PDMA has a much larger molecular weight dependence compared to that of PNIPAM; it can vary from 40 to 50 °C with decreasing molecular weight.[5−7] The LCST of PNIPAM can be finely tuned when they are random or block copolymerized with a hydrophilic or hydrophobic monomer, which will accordingly increase or decrease its LCST. Both *H40* and *H40* macroRAFT agent are water-insoluble, preliminary experiments also reveal that *H40*-PNIPAM with very short PNIPAM graft chains (DP < 20) is also insoluble in water; thus, *H40* core is considered to be hydrophobic. For *H40*-PNIPAM in aqueous solution, there exist hydrogen bonding interactions between the surface carboxyl groups of *H40* core and PNIPAM (Scheme 2), but this will only affect the first few NIPAM repeat units close to *H40*, so hydrogen bonding interactions are not considered.

In LLS studies, the concentration used for *H40*-PNIPAM is 1.0×10^{-6} g/mL to avoid any possible aggregation between dendritic unimolecular micelles above the phase transition temperature of PNIPAM, whereas in micro-DSC characterization, we need to use much higher concentration of 1.0×10^{-3} g/mL to have enough detection sensitivity.

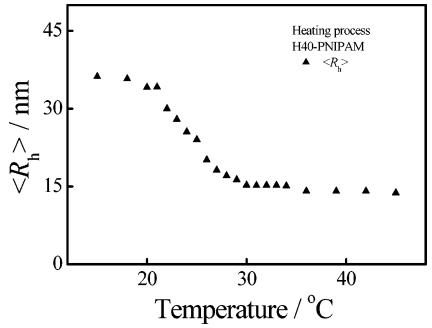

Figure 3. Temperature dependence of the average hydrodynamic radius, $\langle R_h \rangle$, of *H40*−PNIPAM in aqueous solution during the heating process. The concentration is 1.0×10^{-6} g/mL.

Figure 3 shows the temperature dependence of $\langle R_h \rangle$ of *H40*−PNIPAM in aqueous solution. Each data point was obtained after the measured values were stable. For *H40*−PNIPAM, $\langle R_h \rangle$ decreases gradually from 34 to 15 nm in the broad temperature range 20−30 °C, although it is well-known that, for PNIPAM homopolymer chain, $\langle R_h \rangle$ drops quickly in the narrow temperature range 31−33 °C.

When PNIPAM chains are attached by one end to a flat substrate or curved interface (such as latex particles) with a sufficient density, referred to as a polymer brush, they are crowned and forced to stretch away from the solid surface to avoid overlapping. The molecular size of *H40* is estimated to be ca. 3 nm, the grafting of 60 PNIPAM chains from the *H40* core results in a densely packed PNIPAM brush surrounding the hydrophobic core, the grafting density is estimated to be ca. 2 chains/nm^2. Both *H40*−PNIPAM and *H40*−PNIPAM-PDMA can thus be treated as homopolymer or diblock copolymer brush at the surface of the hydrophobic *H40* core.

Theoretical predications suggest that the strong interchain interactions are present in the brush and cause a broadening of the transition of polymer chains.[54−55] Experimental results have already confirmed this predication. Zhu et al. have sterically or electrosterically stabilized PS latex particles with PNIPAM chains with DP of 3000 or 6000. In both cases, dynamic LLS reveals that the grafted PNIPAM layer exhibits a broad phase transition spanning ca. 20 °C, which starts at pretty low temperatures of ca. 15−20 °C, compared to ca. 1−2 °C for that of free PNIPAM chains.[56] Although the grafting density of PNIPAM chains at the latex surface was not reported in this system, it is not expected to be very high. So it is difficult to directly compare their results with ours. Just recently, Tenhu et al.[57] and Zhang et al.[58] have reported thermoresponsive conformational changes of PNIPAM

(54) Zhao, B.; Brittain, W. J. *Prog. Polym. Sci.* **2000**, *25*, 677.
(55) Halperin, A.; Tirrell, M.; Lodge, T. P. *Adv. Polym. Sci.* **1992**, *100*, 31.
(56) Zhu, P. W.; Napper, D. H. *J. Colloid Interface Sci.* **1994**, *164*, 489.
(57) Nuopponen, M.; Ojala, J.; Tenhu, H. *Polymer* **2004**, *45*, 3643.
(58) Zhang, W.; Zhou, X.; Li, H.; Fang, Y.; Zhang, G. *Macromolecules* **2005**, *38*, 909.

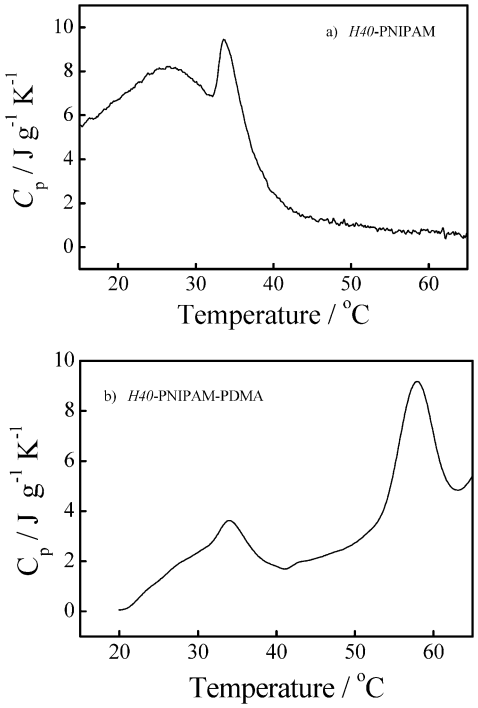

Figure 4. Temperature dependence of partial heat capacity (C_p) of aqueous solution of (a) *H40*−PNIPAM and (b) *H40*−PNIPAM-PDMA at a concentration of 1.0×10^{-3} g/mL. The heating rate is 1.0 °C/min.

chains in the micellar corona assembled from polystyrene-*block*-poly(*N*-isopropylacrylamide) (PS-*b*-PNIPAM), where PS forming the micellar core. They reported that PNIPAM chains in the shell exhibit a broader phase transition in the range 20−36 °C, compared to that of the free PNIPAM chains in water.

We then measured the partial heat capacity (C_p) of *H40*-PNIPAM in aqueous solution using a microcalorimeter. Figure 4a shows the temperature dependence of partial heat capacity (C_p) of aqueous solutions of *H40*-PNIPAM at a concentration of 1.0×10^{-3} g/mL, where the heating rate is 1.0 °C/min. For *H40*-PNIPAM, the micro-DSC curve shows one broad and one sharp endothermic peak located at ∼26 and ∼34 °C, respectively. This suggests the existence of double phase transitions for PNIPAM brush at the dendritic *H40* core. This observation is in agreement with experimental results reported by Tenhu et al. They have grafted PNIPAM brush from gold nanoparticles; the DP of grafted PNIPAM chain is ∼50, and the grafting density is very high, ca. 0.4 nm^2 per chain. Microcalorimetric measurements also reveal two well-separated phase transitions for densely grafted PNIPAM brush at the gold core surface.[59]

Dynamic LLS results of H40−PNIPAM tell us that there exists a broad phase transition ranging from 20 to 30 °C, whereas micro-DSC results reveal double phase transitions with the peaks located at 26 and 34 °C, respectively. This discrepancy may be due to the fact that LLS only probes the entire dendritic *H40*−PNIPAM macromolecules, whereas micro-DSC probes the "local" chain conformations of the PNIPAM brush. It is quite reasonable to postulate that $\langle R_h \rangle$ is not sensitive to the second phase transition at ca. 33 °C.

In our case, PNIPAM brushes are covalently linked to a hydrophobic *H40* core, and it is reasonable to expect that PNIPAM chain segments in the inner and outer part of the brush behave differently due to differences in the extent of chain crowding. Balamurugan et al. used surface plasmon resonance (SPR) spectroscopy and contact angle measurements to study the PNIPAM brush, grafted from a mixed self-assembled monolayer on a bulk gold surface.[60] The SPR results indicated that the PNIPAM brush undergoes a broad transition (over the temperature range 10−40 °C) without abrupt changes, while contact angle measurements, which are more surface sensitive (the outermost 0.5−1 nm) than SPR technique, revealed a sharp change at 32 °C. Based on the results of the polymer brush grafted from a flat surface, we tentatively postulate that the inner layer of the brush collapses first, followed by the collapse of the outer layer of the brush. We are currently respectively labeling the inner or outer part of the PNIPAM brush in *H40*-PNIPAM with pyrene groups; hopefully temperature-dependent excimer fluorescence characterization will reveal the truth.

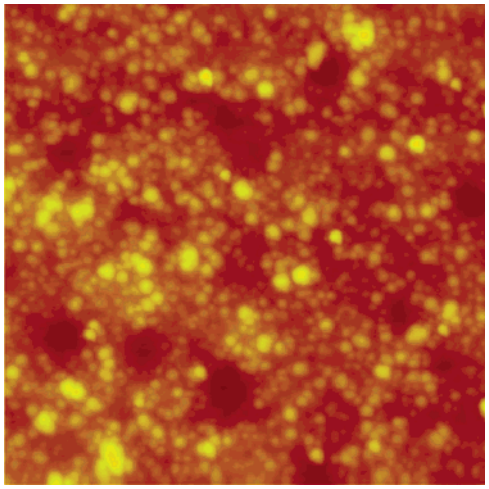

Figure 5. AFM height image (3.5 μm × 3.5 μm) of dendritic *H40*−PNIPAM-PDMA aqueous solution (1.0×10^{-3} g/mL) deposited on mica. The measured heights of all nanospheres are less than 7 nm.

Thermally Induced Collapse and Swelling of *H40*-PNIPAM-PDMA. The morphology of *H40*−PNIPAM-PDMA in aqueous solution is shown in Figure 5. Spherical, randomly distributed nanospheres with diameter ranging from 80 to 140 nm are observed. When *H40*−PNIPAM-PDMA is directly dissolved in water, the solution pH is about 8.4. So about 10% of DMA units in the PDMA corona are positively charged considering that the pK_a of the PDMA homopolymer is ∼7.3,[5] whereas the mica surface is negatively charged. The observed spherical structure appears to be trapped in a solution conformation due to strong attraction of partially positively charged dendritic nanostructures to negatively charged mica substrate. This can partially explain why the nanospheres deposited on mica take a quite flat and extended conformation; the measured heights of all the nanospheres are less than 7 nm, much smaller than the nanosphere diameter. Although we do not observe the core−shell structure from the AFM height image, from a structural point of view, *H40*−PNIPAM-PDMA in aqueous solution will take a unimolecular three-layer core−shell-corona conformation, with hydrophobic *H40* as the core, thermoresponsive PNIPAM as the inner layer, and thermoresponsive PDMA as the corona. So *H40*−PNIPAM-PDMA in aqueous solution can be treated as spherical unimolecular micelles, with two different thermoresponsive shells. A schematic illustration is shown in Scheme 3.

LLS Characterization. Dendritic *H40*-PNIPAM-PDMA has two different thermoresponsive layers. PNIPAM and PDMA homopolymers undergo phase transitions at their LCST, which are found to be 32 °C for PNIPAM and 40−50 °C for PDMA,[5−7]

(59) Shan, J.; Chen, J.; Nuopponen, M.; Tenhu, H. *Langmuir* **2004**, *20*, 4671.

(60) Balamurugan, S.; Mendez, S.; Balamurugan, S. S.; O'Brien, M. J.; Lopez, G. P. *Langmuir* **2003**, *19*, 2545.

Scheme 3. Schematic Illustration of the Thermally Induced Collapse of *H40*-PNIPAM-PDMA upon Heating through the LCSTs of PNIPAM and PDMA

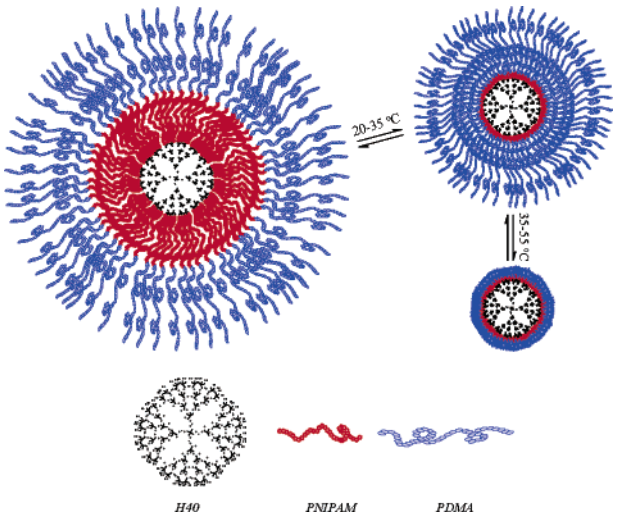

respectively. Upon heating, *H40*-PNIPAM-PDMA is expected to exhibit double thermoresponsive collapse at phase transition temperatures of the PNIPAM inner layer and PDMA outer layer.

In LLS characterization of *H40*-PNIPAM-PDMA, a concentration of 1.0×10^{-6} g/mL was used again to avoid any possible aggregation above the phase transition temperature of the PDMA outer corona. It should be noted that below the phase transition temperature of PDMA layer, the phase transition of the inner PNIPAM layer is expected not to cause any intermicellar aggregation due to the screening of the soluble PDMA outer corona.

Figure 6 shows typical angular dependences of the Rayleigh ratio $[KC/R_{vv}(q)]$ of *H40*-PNIPAM-PDMA at three different temperatures (15, 35, and 60 °C), which are below the LCST of PNIPAM, above the LCST of PNIPAM, but below the LCST of PDMA, and above the LCST of PDMA block. dn/dC values determined at the corresponding temperatures are used. On the basis of eq 1, with increasing temperature, the slope decreases, reflecting the decrease of $\langle R_g \rangle$, i.e., the shrinking of the grafted PNIPAM-*b*-PDMA chains. The extrapolation of $KC/R_{vv}(q)$ to $q \rightarrow 0$ at three different temperatures leads to almost the same intercept (±5%), indicating that the weight-average molar mass ($M_{w,app}$) is constant during the shrinking process. So for the heating process, what we observe for the shrinking PNIPAM inner layer and PDMA outer corona involves only unimolecular processes.

Figure 7 summarizes the temperature dependence of $\langle R_g \rangle$ and $\langle R_h \rangle$ of *H40*−PNIPAM-PDMA during one cycle of the heating-and-cooling process. During the heating process, a two-stage

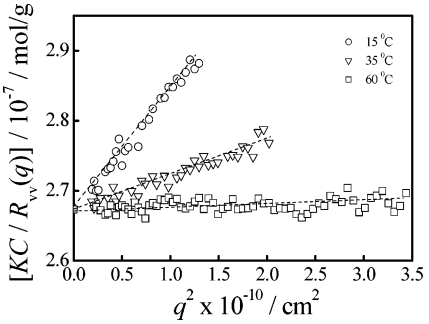

Figure 6. Scattering vector (q) dependence of Rayleigh ratio $R_{vv}(q)$ of dendritic macromolecules *H40*−PNIPAM-PDMA in water, where the concentration is 1.0×10^{-6} g/mL.

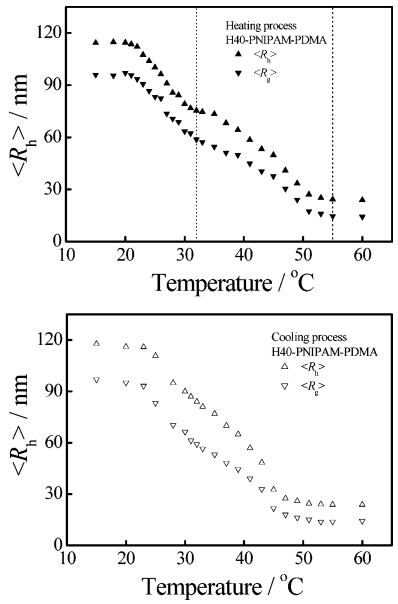

Figure 7. Temperature dependence of the average radius of gyration, $\langle R_g \rangle$, and the average hydrodynamic radius, $\langle R_h \rangle$, of *H40*−PNIPAM-PDMA during one cycle of heating-and-cooling process. The concentration of aqueous solution of *H40*−PNIPAM-PDMA is 1.0×10^{-6} g/mL.

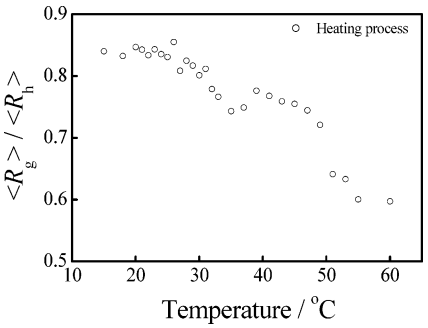

Figure 8. Temperature dependence of the ratio of the average radius of gyration to the average hydrodynamic radius, $\langle R_g \rangle/\langle R_h \rangle$, of *H40*−PNIPAM-PDMA during the heating process. The concentration is 1.0×10^{-6} g/mL.

collapse can be clearly seen. At a lower temperature (15−20 °C), water is a good solvent for both PNIPAM and PDMA blocks, and dendritic macromolecules in water exist in a three-layer core−shell−corona conformation with hydrophobic *H40* as the core, swollen PNIPAM as the inner shell, and swollen PDMA as the corona.

Compared to *H40*−PNIPAM (Figure 3), the decrease of $\langle R_h \rangle$ from 115 to 75 nm in the temperature range 20−32 °C should be ascribed to the collapse of the PNIPAM inner shell. There is a small plateau of $\langle R_h \rangle$ in the range 32−36 °C, although the decrease from 73 to 24 nm in the range 36−55 °C should be due to the collapse of PDMA corona. At temperatures higher than 55 °C, $\langle R_h \rangle$ reaches another plateau.

We also plotted the temperature dependence of the ratio $\langle R_g \rangle/\langle R_h \rangle$ that reflects the chain density distribution (Figure 8). It again reveals a two-stage decrease, corresponding to the phase transition of the PNIPAM inner layer and PDMA outer layer, respectively. The fact that, at lower temperatures of 15−20 °C, $\langle R_g \rangle/\langle R_h \rangle \sim 0.85$ can be attributed to the stretched conformation of PNIPAM and PDMA blocks due to chain crowding in the diblock copolymer brush. The decrease of $\langle R_g \rangle/\langle R_h \rangle$ from 0.85 at 15−20 °C to 0.74 at 35 °C clearly reveals the collapse of the PNIPAM inner shell, which leads to a denser core. Although R_h

and R_g both show a continuous decrease from 20 to 32 °C, the biggest drop of $\langle R_g \rangle / \langle R_h \rangle$ takes place in the temperature range 25−35 °C. We can also observe a small dip of $\langle R_g \rangle / \langle R_h \rangle$ around 35 °C. A careful reexamination of Figure 7 tells us that the dip is due to the fact that $\langle R_h \rangle$ keeps nearly constant in the range 32−35 °C, whereas $\langle R_g \rangle$ keeps decreasing in the same temperature range.

Upon further increasing the temperature, the PDMA layer will undergo phase transition and collapse. Both $\langle R_g \rangle$ and $\langle R_h \rangle$ show almost synchronized decrease, and then stabilize above 55 °C (Figure 7). $\langle R_g \rangle / \langle R_h \rangle$ further decreases in the temperature range 39−55 °C, and then stabilizes at 0.60 above 55 °C (Figure 8). The biggest drop in $\langle R_g \rangle / \langle R_h \rangle$ value takes place at around 50 °C. Unlike the collapse of the PNIPAM layer, we do not observe a dip in $\langle R_g \rangle / \langle R_h \rangle$ during the collapse of the PDMA layer. It is helpful to note that for a uniform solid sphere, $\langle R_g \rangle / \langle R_h \rangle \sim 0.774$. Core−shell nanostructures with nonuniform density distributions, i.e., quite dense core and looser shell, can have such low $\langle R_g \rangle / \langle R_h \rangle$ values.[61] During the coil-to-globule transition of a single PNIPAM chain, the experimental $\langle R_g \rangle / \langle R_h \rangle$ value can be as low as 0.62 in the collapsing limit.[48] The lower $\langle R_g \rangle / \langle R_h \rangle$ value of 0.60 at 55−60 °C suggests that even at such high temperatures, which are much larger than the LCST of PDMA homopolymer with similar DP, the PDMA outer corona is not fully collapsed. This is highly possible considering that the phase transition of polymer brush is expected to be broadened to a large extent, and the chain crowding in the polymer brush resists completely collapsing at comparable temperatures for the fully collapsed free polymer chains.

Figure 7 also shows the temperature dependence of $\langle R_g \rangle$ and $\langle R_h \rangle$ during the cooling process. A two-stage reswelling is clearly evident. Although the heating and cooling processes are generally reversible, these two processes do not strictly superimpose; there exists a hysteresis. The temperature dependence of $\langle R_g \rangle$ and $\langle R_h \rangle$ is somewhat flatter in the cooling process than that in the heating process. At temperatures lower than 20 °C, water becomes a good solvent for both PNIPAM and PDMA, and $\langle R_g \rangle$ and $\langle R_h \rangle$ during the cooling and heating process coincide to each other, indicating that both PNIPAM and PDMA are now completely reswollen.[61]

It should be noted that, during the heating and cooling processes for LLS studies, each data point was obtained after the measured values were stable; it generally takes ∼30−40 min for equilibration at each temperature. LLS experiments from two cycles of the heating-and-cooling process give repeatable temperature dependence of $\langle R_g \rangle$ and $\langle R_h \rangle$ within experimental error during the heating and cooling processes; that is, the same hysteresis is observed. This hysteresis hints the existence of slow chain rearrangements.

A schematic illustration of the whole thermoresponsive collapsing process of *H40*−PNIPAM-PDMA is shown in Scheme 3. It should be noted that pictures shown in Scheme 3 may not reflect the real microstructures of *H40*−PNIPAM-PDMA, but they would rather be considered as highly simplified and idealized cartoons. Likos et al. have concluded in a recent review that hyperbranched polymers or dendrimers exhibit a dense-core structure in which the terminal groups are partially folded back; thus, flexible dendrimers do not have a well-defined surface or interior.[62] In describing the real structure, we should also consider the chain length distribution of PNIPAM and PDMA blocks. Furthermore, the collapsing of PNIPAM and PDMA layers is actually a very complex process. The collapse of the PNIPAM inner layer (even for H40−PNIPAM, it exhibits double phase transitions) will inevitably increase the chain density of PDMA at the PNIPAM/PDMA interface. To be more accurate, the collapsing of any chain segments in the diblock copolymer brush will affect the collapse of un-collapsed chain segments. All of the above three points will lead to a smearing of the interface between different regions.

Micro-Differential Scanning Calorimetry (Micro-DSC). We also measured the partial heat capacity, C_p, of *H40*−PNIPAM-PDMA in aqueous solution using a microcalorimeter. Compared to that for LLS studies, a much higher concentration of 1.0×10^{-3} g/mL was used in micro-DSC to have enough detection sensitivity. At this concentration, light scattering intensity at a scattering angle of 15° keeps constant in the temperature range 20−30 °C. It then increases 10−20% in the range 35−60 °C, accompanied by the appearance of bimodal distribution of R_h, the peaks of which are located at 76 and 210 nm, respectively. The above observations suggest partial aggregation between dendritic *H40*-PNIPAM-PDMA macromolecules at a concentration of 1.0×10^{-3} g/mL. Figure 4b reveals two endothermic peaks located at 34 and 58 °C, respectively. The first broad peak extends from 20 to 40 °C with a shoulder located at around 26 °C, and this is quite comparable to that of *H40*−PNIPAM. The first broad endothermic peak can be easily ascribed to the phase transition of the PNIPAM inner layer. This peak also generally correlates with the LLS results, where $\langle R_h \rangle$ and $\langle R_g \rangle$ continuously decrease in this temperature range. Around the peak temperature of ca. 34 °C, $\langle R_h \rangle$ stabilizes, $\langle R_g \rangle$ is still decreasing, and $\langle R_g \rangle / \langle R_h \rangle$ shows a local minimum (Figures 7 and 8).

The second endothermic peak at 58 °C should be ascribed to the phase transition of PDMA outer corona. Both $\langle R_g \rangle$ and $\langle R_h \rangle$ cease to decrease above 55 °C, and the biggest drop of $\langle R_g \rangle / \langle R_h \rangle$ takes place around 50 °C (Figures 7 and 8). This discrepancy may be due to the difference in detection principles: LLS only probes the entire dendritic *H40*−PNIPAM macromolecules, but it cannot differentiate between the PNIPAM inner shell and PDMA corona, whereas micro-DSC probes "local" chain conformations of PNIPAM and PDMA layers at different temperatures. As discussed in a previous section, the microstructure of *H40*−PNIPAM-PDMA is very complex; it is highly possible that well-segregated PNIPAM and PDMA layers may even not exist. Furthermore, a much higher concentration is used for micro-DSC studies; there exist partial aggregation between dendritic *H40*-PNIPAM-PDMA macromolecules. All of these will lead to discrepancies in the phase transition temperatures obtained from LLS and micro-DSC.

Excimer Fluorescence Measurements. Pyrene has been widely used as a probe of structure and dynamics in macromolecular systems because of its long excited-state lifetime and spectral sensitivity to the surrounding medium.[63,64] Excimer fluorescence measured by the excimer-to-monomer ratio (I_e/I_m) provides highly localized information because the excimer is only formed when aromatic rings closely approach each other within 4−5 Å. Here we selectively labeled the PDMA outer layer of *H40*−PNPAM-PDMA dendritic macromolecules with pyrene (we denote it *H40*−PNIPAM-PDMA(Py)). The fluorescence spectra of aqueous *H40*−PNIPAM-PDMA(Py) at different temperatures were shown in Figure 9. Besides the monomer bands that are characteristic of the pyrene vibronic structure, three distinct peaks located at 373, 393, and 415 nm, respectively, the excimer emission of pyrene appears as a broad, structureless band around 480 nm.

(61) Chen, H. W.; Li, J. F.; Ding, Y. W.; Zhang, G. Z.; Zhang, Q. J.; Wu, C. *Macromolecules* **2005**, *38*, 4403.
(62) Likos, C. N.; Ballauff, M. *Top Curr. Chem.* **2005**, *245*, 239.
(63) Chen, W.; Durning, C. J.; Turro, N. J. *Macromolecules* **1999**, *32*, 4151.
(64) Kalyanasundaram, K.; Thomas, J. K. *J. Am. Chem. Soc.* **1977**, *99*, 2039.

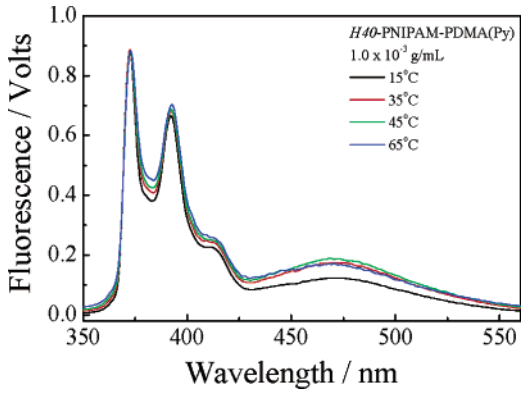

Figure 9. Normalized fluorescence spectra of aqueous solution of *H40*−PNIPAM-PDMA(Py) (1.0×10^{-3} g/mL) at different temperatures.

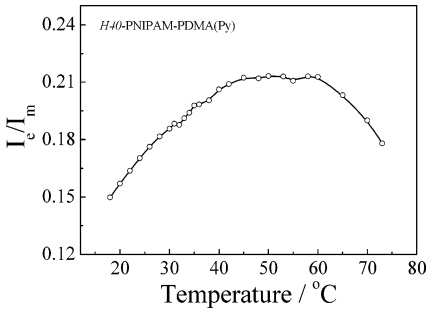

Figure 10. Variation of excimer-to-monomer intensity ratio, I_e/I_m, for *H40*−PNIPAM- PDMA(Py) in aqueous solutions (1.0×10^{-3} g/mL) as a function of temperature.

The spectral parameter of interest to us is the excimer (around 480 nm) to monomer (373 nm) intensity ratio (I_e/I_m).

Figure 10 depicts the temperature dependence of I_e/I_m for aqueous solutions of *H40*−PNIPAM-PDMA. It is interesting to observe that I_e/I_m first gradually increases in the range 18−40 °C, reaches a plateau in the range 40−60 °C, and then decreases above 60 °C. The first impression we get by comparing excimer fluorescence results to the micro-DSC results is that they agree with each other to some extent. The first phase transition of PNIPAM detected by micro-DSC finished at about 40 °C. The increase of I_e/I_m in the range 18−40 °C is due to the chain stretching of PDMA(Py), resulting from the collapse of the PNIPAM inner layer and the simultaneous increase of chain density of PDMA at the PNIPAM/PDMA interface. On average, there are 2.2 pyrene groups per PDMA chain. Stretched PDMA-(Py) chains render pyrene groups located on neighboring PDMA chains to come close in proximity, although it will be less likely for pyrene groups from the same PDMA chain to come close to each other if the chains are more stretched.[34,65−66] These two processes will compete to determine the change of I_e/I_m values.

For the I_e/I_m plateau range of 40−60 °C, we tentatively ascribed it to the collapsing range of the PDMA layer. The PDMA homopolymer is a very viscous solid with lower glass transition temperature (T_g) as compared to that of PNIPAM, although PDMA chains within an isolated dendritic nanostructure can collapse and aggregate into an oily layer, but still with considerable chain mobility. At temperatures above 60 °C, I_e/I_m decreases with increasing temperature. Micro-DSC results shown in Figure 4b exhibit a second phase transition peak at 58 °C. The drop in I_e/I_m above 60 °C could be due to the further collapse of the PDMA outer layer; now PDMA is more hydrophobic, the mobility of chains as well as linked chromophores is greatly restrained, and they get fewer chances to come close to each other.[65,66]

Conclusion

Double phase transitions of unimolecular dendritic core−inner-shell−corona nanostructures with dual thermoresponsive coronas were studied. Two successive reversible addition-fragmentation transfer (RAFT) polymerizations of NIPAM and DMA were conducted at the periphery of *H40* macroRAFT agent to prepare *H40*−PNIPAM-PDMA. The resulting dendritic unimoelcular micelles exhibit two-stage thermoresponsive collapse or re-swelling upon heating or cooling, this was confirmed by LLS, micro-DSC, and excimer fluorescence measurements. These four techniques are complementary and all support the double phase transition behavior.

Acknowledgment. This work is supported by an Outstanding Youth Fund (50425310) and a key research grant (20534020) from the National Natural Scientific Foundation of China (NNSFC) and the "Bai Ren" Project of the Chinese Academy of Sciences.

LA0522707

(65) Winnik, F. M. *Macromolecules* **1990**, *23*, 233.
(66) Picarra, S.; Duhamel, J.; Fedorov, D. A.; Martinho, J. M. G. *J. Phys. Chem. B* **2004**, *108*, 12009.